Supporting Information

Interface Engineering Assisted 3D-Graphene/Germanium Heterojunction for High-Performance Photodetectors

Menghan Zhao,[†,&] Zhongying Xue,[‡,&] Wei Zhu,[†] Gang Wang,[†,*] Shiwei Tang,[†] Zhiduo Liu,[‖] Qinglei Guo[#], Da Chen,[†] Paul K. Chu,[§] Guqiao Ding,[‡] and Zengfeng Di[‡,*]

[†]*Department of Microelectronic Science and Engineering, School of Physical Science and Technology, Ningbo University, Ningbo 315211, P. R. China*

[‡]*State Key Laboratory of Functional Materials for Informatics, Shanghai Institute of Microsystem and Information Technology, Chinese Academy of Sciences, Shanghai 200050, P. R. China*

[‖]*State Key Laboratory of Integrated Optoelectronics, Institute of Semiconductors, Chinese Academy of Sciences, Beijing 100083, P. R. China*

[§]*Department of Physics, Department of Materials Science and Engineering, and Department of Biomedical Engineering, City University of Hong Kong, Tat Chee Avenue, Kowloon, Hong Kong 999077, P. R. China*

[#]*Center of Nanoelectronics and School of Microelectronics, Shandong University, Jinan 250100, P. R. China*

[&]*Both authors have contributed equally to this work*

*Corresponding Authors

E-mail: gangwang@nbu.edu.cn;

E-mail: zfdi@mail.sim.ac.cn;

1. Synthesis of 3D-Gr/2D-Gr/Ge

A Ge wafer (110) was placed at the center of the horizontal quartz tube (60 mm inner diameter) and evacuated to a base pressure of about 0.1 Pa. Argon (99.9999% pure) and hydrogen (99.9999% pure) were bled at rates of 200 sccm (standard cubic cm per min) and 25 sccm, respectively, to reach atmospheric pressure. The 2D-Gr was deposited on Ge at 910 ^{o}C for 200 min in Ar, H_2, and methane (CH_4) (200 : 25 : 0.5 sccm). After the reaction, the gases were shut off and the furnace cooled to the predesignated temperature from 450 ^{o}C to 600 ^{o}C. The quartz tube was then evacuated to approximately 3 Pa and CH_4 (5 sccm) was introduced for different time (10 min to 40 min) to produce 3D-Gr, distances (from 16 cm to 34 cm), and power (60 W to 150 W). After the reaction, the plasma power was turned off, gas flow was shut off, and furnace cooled to room temperature under flowing Ar. The process is summarized in Figure S1.

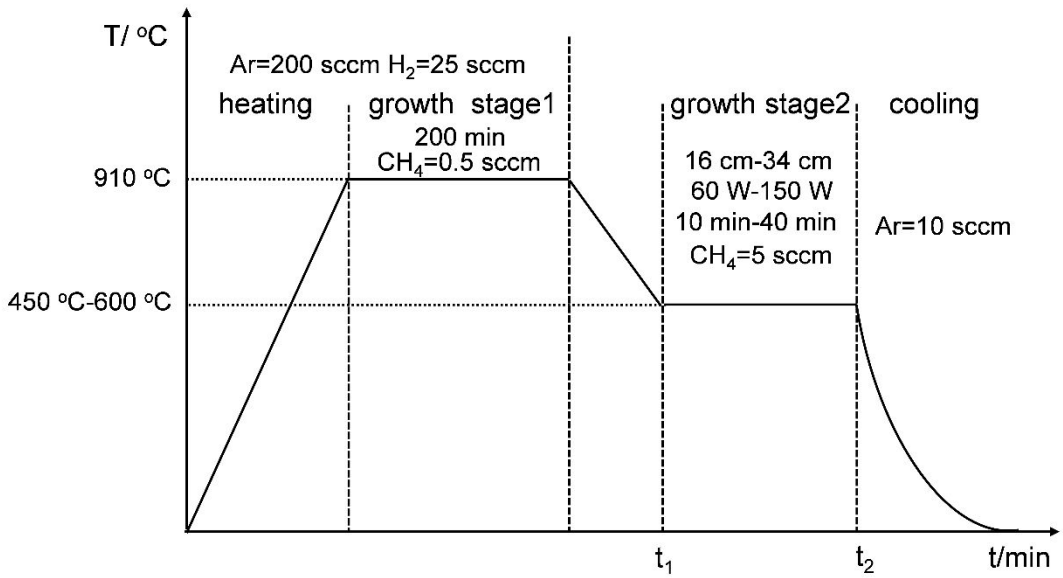

Figure S1. Schematic illustration of the synthesis of 3D-Gr/2D-Gr/Ge.

The monolayer feature and high crystallinity of the 2D-graphene (2D-Gr) is confirmed by transmission electron microscopy (TEM) and selected area electron diffraction (SAED), which was transferred from the Ge substrates onto TEM grids, as shown in Figure S2. The suspended 2D-Gr on the TEM grids are continuous over a large area, as shown in Figure S2(a). In order to further investigate microscopic structure, the 2D-Gr is characterized by high resolution TEM (HRTEM). Figure S2(b) displays the microscopic structures of the 2D-Gr and a typical honeycomb lattice structure is observed. The HRTEM image shows few to no defects in a range greater than 100 nm^2, indicating the high crystalline quality of the 2D-Gr.[1] The SAED pattern of the 2D-Gr is displayed in Figure S2(c). Only one set of hexagonal diffraction pattern is observed and a single crystalline lattice structure can be inferred.[2] And the band intensity ratio (outermost to innermost) of ~1:2 (Figure S2(d)) suggests the formation of single-layer graphene.[3]

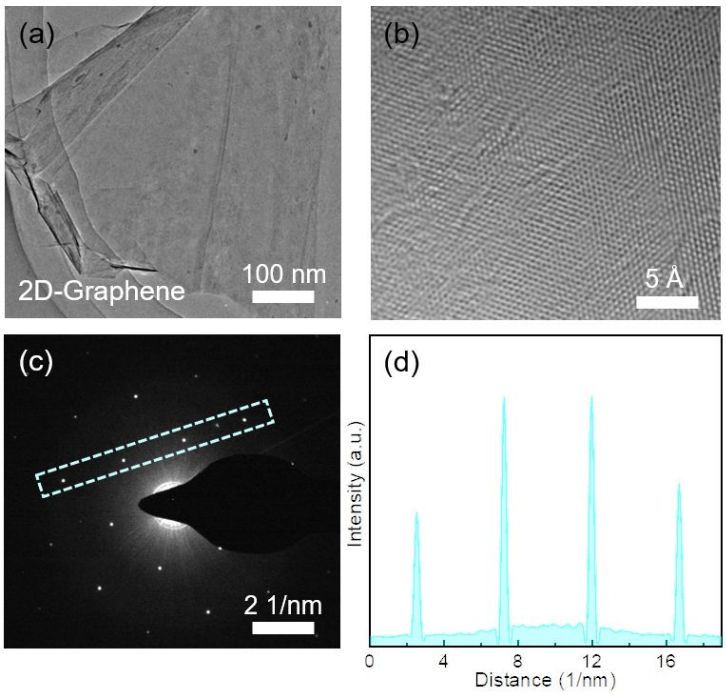

Figure S2. (a) Low-resolution TEM image showing 2D-Gr suspended on a TEM grid.

(b) HRTEM image of the 2D-Gr. (c) SAED pattern of the 2D-Gr. (d) Profile of diffraction spot intensities along box in (c).

2. Experimental parameters of 3D-Gr/2D-Gr/Ge

The plasma power shows critical effects on the vertical growth of the 3D-Gr as verified by the Raman spectra in Figure S3(a) which shows that the quality of 3D-Gr improves with power. A large defect-related D peak appears at around 1350 cm^{-1} and $I_D/I_G \approx 1.76$, indicating the presence of defects in 3D-Gr (Figure S3(b)). It decreases from 1.76 to 1.07 when the plasma power is increased from 30 to 150 W, meaning that both the amount of precipitated carbon atoms and defects in 3D-Gr decrease as the plasma power is increased. The cross-sectional SEM images in Figure S3(c-f) suggest that the heights of 3D-Gr vary from 130 nm to 350 nm as the plasma power is increased.

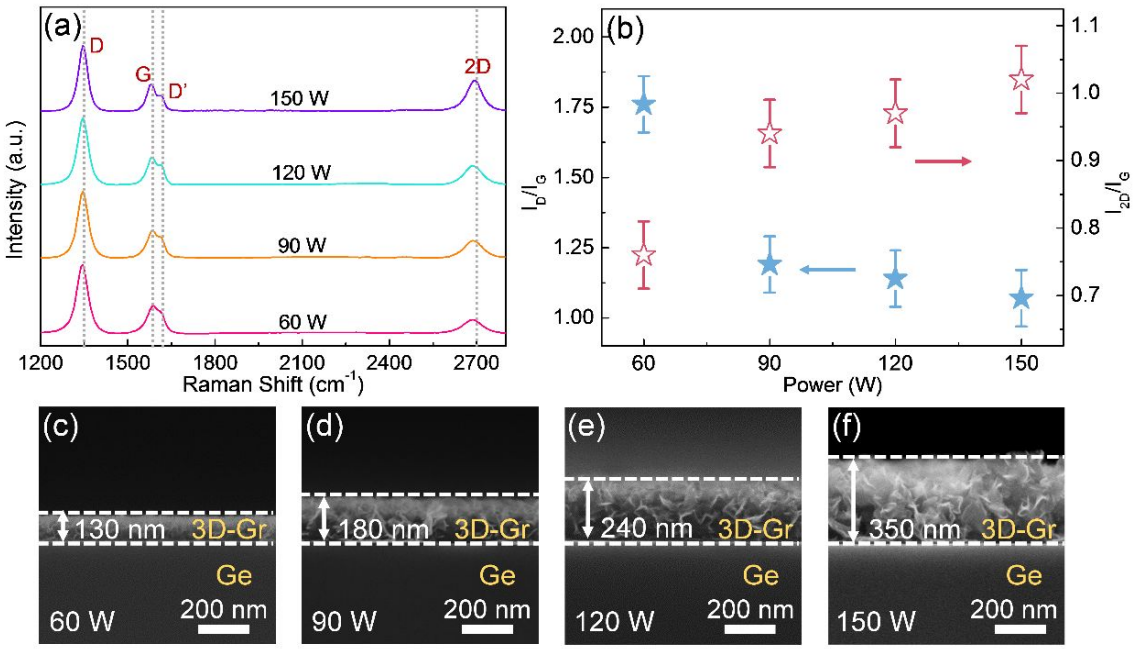

Figure S3. (a) Raman scattering spectra of 3D-Gr deposited on 2D-Gr/Ge using

different plasma power. (b) I_D/I_G and I_{2D}/I_G. (c to f) Cross-section SEM images of 3D-Gr fabricated directly on 2D-Gr/Ge with plasma power of 60 W, 90 W, 120 W and 150 W, respectively.

Figure S4(a) shows the Raman scattering spectra of 3D-Gr prepared at different temperature (450-600 °C) and the corresponding I_D/I_G and I_{2D}/I_G values are summarized and plotted in Figure S4(b). The intensity ratio of I_D/I_G decreases gradually from 1.94 to 1.07 while I_{2D}/I_G increases gradually from 0.2 to 1.02 when the temperature is increased from 450 °C to 600 °C. The quality improvement of 3D-Gr with fabrication temperature is further confirmed by the SAED patterns shown in Figure S4(c-f).

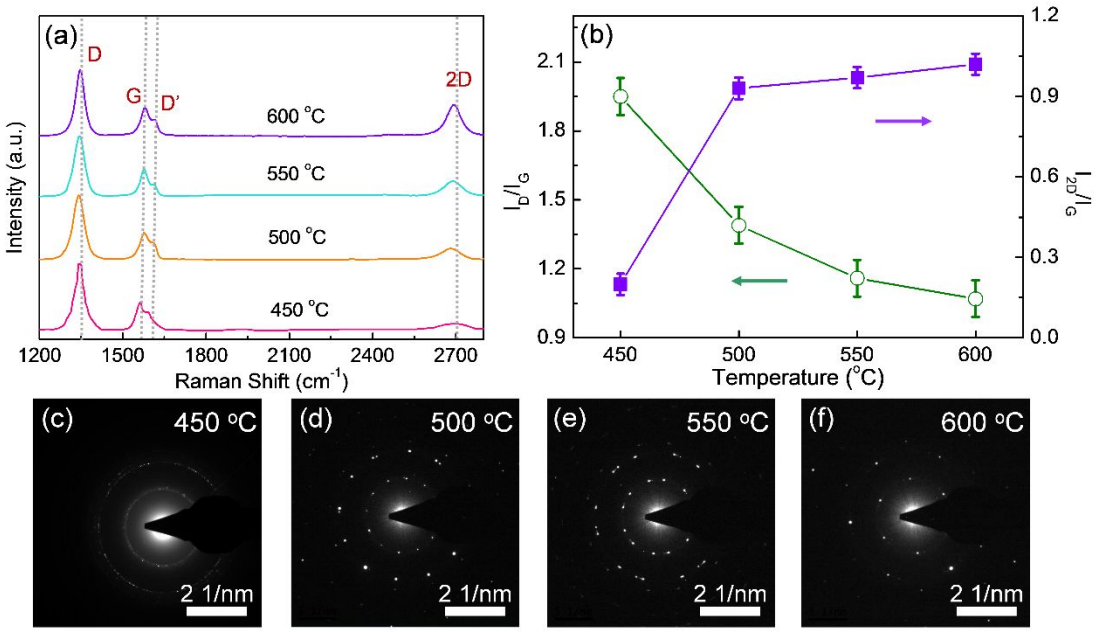

Figure S4. (a) Raman scattering spectra of the 3D-Gr deposited on 2D-Gr/Ge at different temperature. (b) I_D/I_G and I_{2D}/I_G. (c to f) SAED patterns of 3D-Gr fabricated directly on 2D-Gr/Ge at 450 °C, 500 °C, 550 °C, and 600 °C, respectively.

Figure S5(a) displays the Raman spectra of 3D-Gr for different time under the optimal conditions. After 10 minutes, a significant defect-related D peak emerges near 1350 cm^{-1} and $I_D/I_G \approx 1.94$. As the deposition time is increased to 40 min, the defect-related D peak weakens gradually. The intensity ratios of I_D/I_G and I_{2D}/I_G decrease gradually from 1.94 to 1.07 and increase from 0.51 to 1.02, respectively, as the time is increased as shown in Figure S5(b). To assess the quality of Gr in 3D-Gr, Figure S5(c-f) depict the SEM images and Raman maps taken from a relatively large central area of the 3D-Gr surface. Expansion of the 3D-Gr region is indicated by the color-coded intensity maps of I_D/I_G and I_{2D}/I_G over an area of 10 × 10 μm^2. The pink regions correspond to crystalline quality of 3D-Gr and red regions represent defects in 3D-Gr.

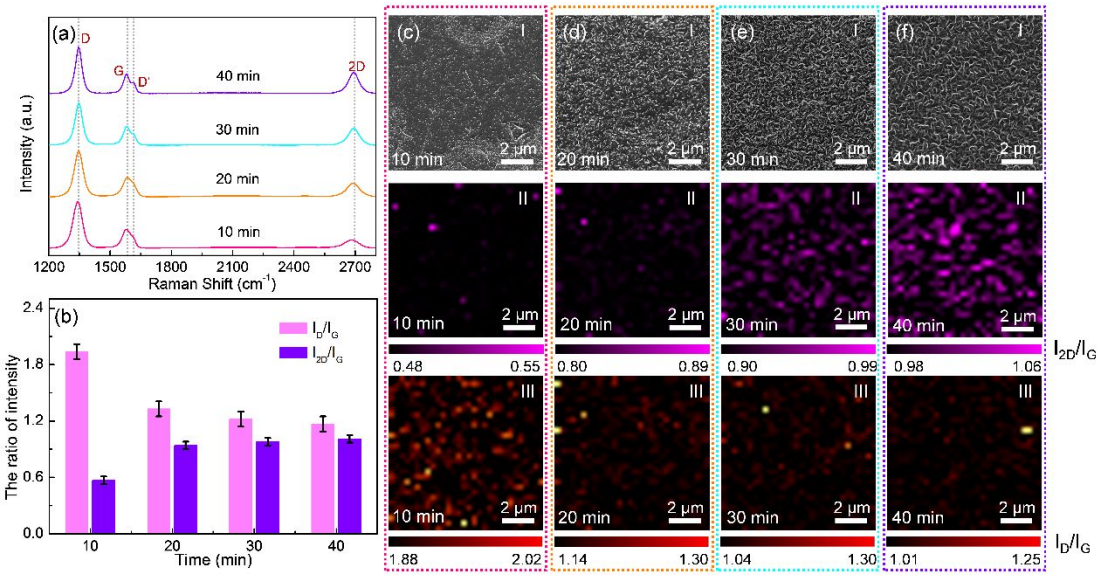

Figure S5. (a) Raman scattering spectra of 3D-Gr deposited on 2D-Gr/Ge for different time under optimal conditions. (b) I_D/I_G and I_{2D}/I_G. (c to f) SEM images and color-coded Raman maps of I_D/I_G and I_{2D}/I_G in 3D-Gr for processing time of 10, 20,

30, and 40 min.

The Raman scattering spectra of 3D-Gr placed at different distances from the plasma source are exhibited in Figure S6(a). Larger crystallite sizes are observed from the films produced at a smaller distance (closer) as shown in Figure S6(b). This relationship indicates improved crystallinity (I_{2D}/I_G from 0.73 to 1.02) when the samples are closer to the plasma source (Figure S3). Figure S6(c-f) present the morphology of the different 3D-Gr samples and the density of vertical sheets decreases with distance. Moreover, a big increase in the growth rate is found as the distance is reduced from 34 to 16 cm (white line in these figures). At shorter distances, the substrate is subjected to a larger electric field and more carbon species can reach the surface without significant recombination.

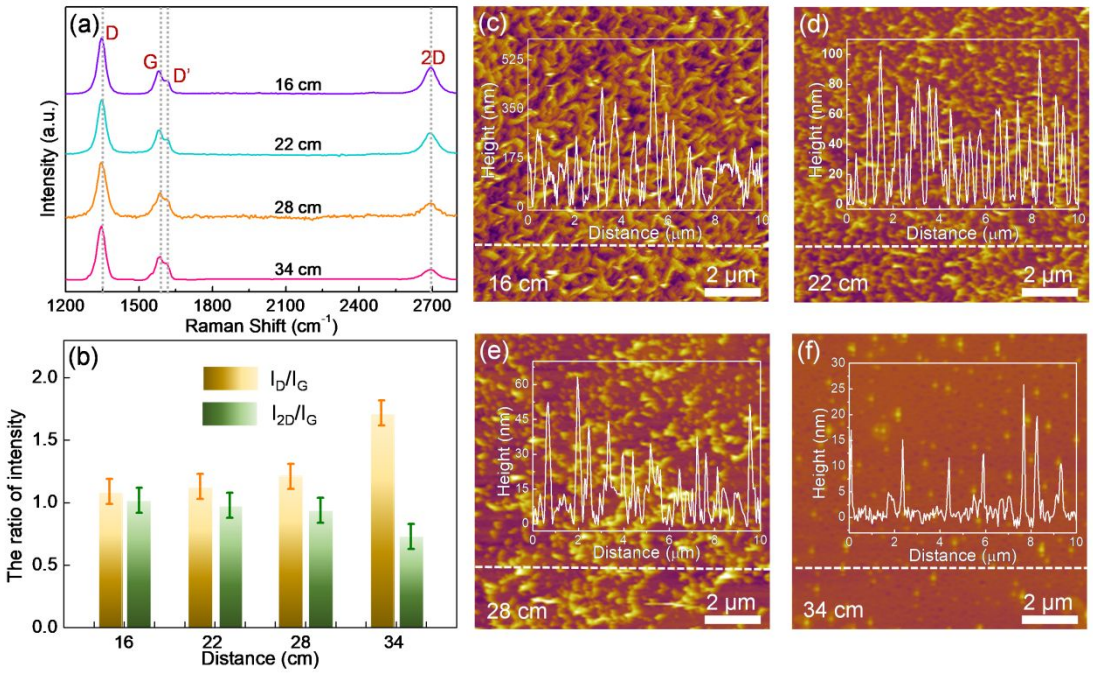

Figure S6. (a) Raman scattering spectra of 3D-Gr deposited on 2D-Gr/Ge at different distances from the plasma source under optimal conditions. (b) I_D/I_G and I_{2D}/I_G. (c to

f) AFM images of 3D-Gr produced directly on 2D-Gr/Ge at distances of 16, 22, 28, and 34 cm, respectively. The corresponding histograms are shown in the inset.

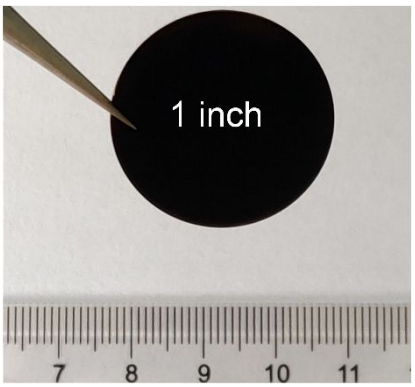

Figure S7. Optical picture of the 1 inch 3D-Gr/2D-Gr/Ge.

3. Chemical composition and chemical states of 3D-Gr/2D-Gr/Ge

XPS was performed to determine the surface chemical composition and chemical states of 3D-Gr on 2D-Gr/Ge and the results are displayed in Figure S8(a). Intrinsic Ge, carbon (C), and oxygen (O) signals are observed. Figure S8(b) shows the high-resolution C 1s spectrum revealing the dominant sp^2 peak and minor sp^3 peak. The sp^2 C originates from sp^2 bonding in graphene and sp^3 C is related to the degree of the graphitization or structural defects of graphene.[4-5]

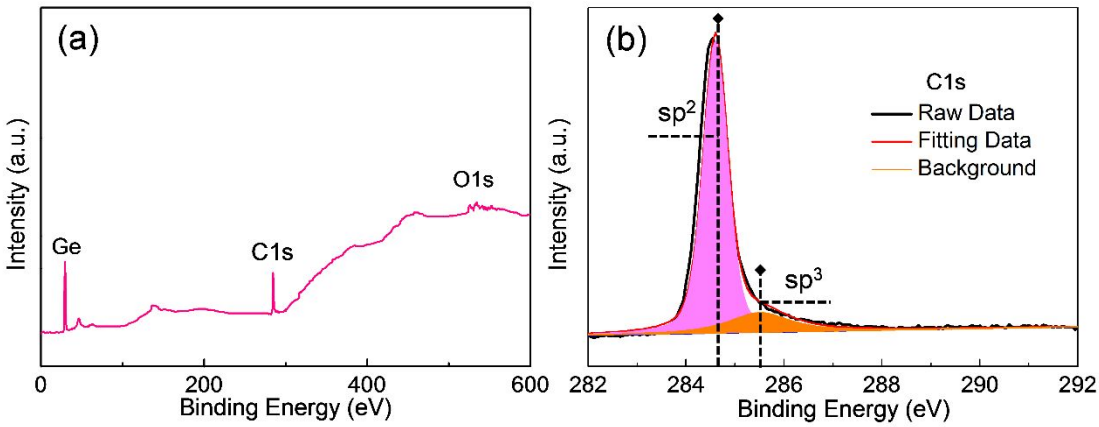

Figure S8. (a) XPS spectrum of 3D-Gr/2D-Gr/Ge. (b) C 1s XPS spectrum of

3D-Gr/2D-Gr/Ge.

4. Photoelectrical measurements of the 3D-Gr/2D-Gr/Ge Schottky junctions

To determine the photoelectrical properties of 3D-Gr/2D-Gr/Ge, electrodes were prepared by deposition of Ag (200 nm) by electron beam evaporation. The photodetectors were characterized under ambient conditions by the Agilent (B1500A) semiconductor parameter analyzer and Keithley 4200 semiconductor characterization system. The responsivity (R) and specific detectivity (D^*) are the key figure-of-merit parameters of a photodetector. R is the physical quantity that reflects the photoelectric conversion capability of the device and D* represents the sensitivity and performance of a detector, which can be expressed by the follow equations:[6-8]

$$R = \frac{I_p}{P_{opt}} = \eta\left(\frac{q\lambda}{hc}\right)G \text{ and} \quad (1)$$

$$D^* = \frac{R}{(2q \cdot I_{dark}/A)^{1/2}} \quad (2)$$

where I_p, P_{opt}, η, h, c, λ, A, q, I_{dark}, and G are the photocurrent, incident light power, quantum efficiency, Planck's constant, speed of light, light wavelength, active area, elementary charge, dark current, and photoconductive gain, respectively.

5. Uniformity and repeatability of the device

To evaluate the uniformity and repeatability, more than twenty 3D-Gr/2D-Gr/Ge Schottky junctions were tested. According to the I_{ds}-V_{ds} curves collected from 6 representative devices shown in Figure S9(a), the rectification behavior is observed from all the photodetectors constructed on the 3D-Gr/2D-Gr/Ge Schottky junction and

the rectification ratios are quite similar. For photocurrents collected at V_{ds} = 1 V from 21 individual photodetectors, the photocurrent histogram reveals that the majority of photocurrent is in the range from 2.3 to 2.7 mA with an average of 2.5 mA (Figure S9(b)), indicating that the photodetector devices constructed on the 3D-Gr/2D-Gr/Ge Schottky junction have excellent reproducibility.

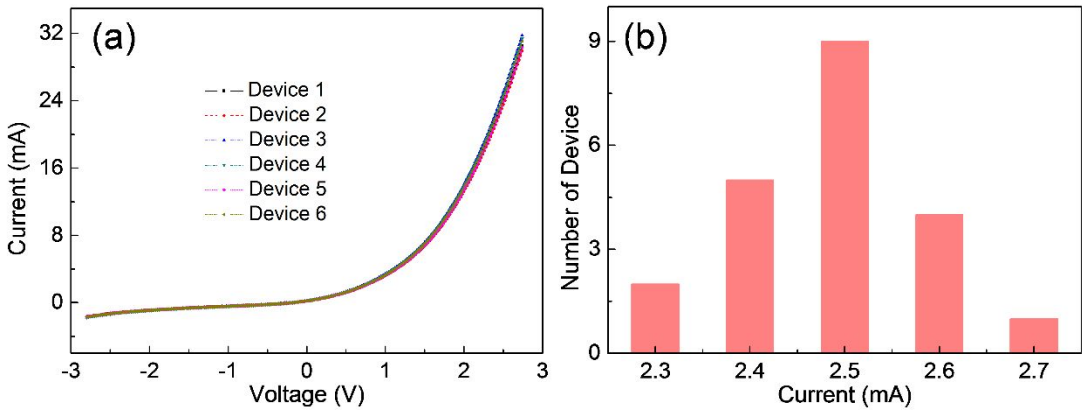

Figure S9. (a) I_{ds}-V_{ds} characteristics of 6 representative photodetectors illuminated with 1,550 nm light (30 mW/cm^2). (b) Histogram of the photocurrents measured at V_{ds} = 1 V for 21 devices.

REFERENCES

(1) Hashimoto, A.; Suenaga, K.; Gloter, A.; Urita, K.; Iijima, S. Direct Evidence for Atomic Defects in Graphene Layers. *Nature* **2004**, *430*, 870–873.

(2) Wang, G.; Zhang, M.; Liu, S.; Xie, X.; Ding, G.; Wang, Y.; Chu, P. K.; Gao, H.; Ren, W.; Yuan, Q.; Zhang, P.; Wang, X.; Di, Z. Synthesis of Layer-Tunable Graphene: A Combined Kinetic Implantation and Thermal Ejection Approach. *Adv. Funct. Mater.* **2015**, *25*, 3666–3675.

(3) Sun, Z.; Raji, A. R. O.; Zhu, Y.; Xiang, C.; Yan, Z.; Kittrell, C.; Samuel, E. L. G.;

Tour, J. M. Large-Area Bernal-Stacked Bi-, Tri-, and Tetralayer Graphene. *ACS Nano* **2012**, *11*, 9790–9796.

(4) Yang, C.; Bi, H.; Wan, D.; Huang, F.; Xie, X.; Jiang, M. Direct PECVD Growth of Vertically Erected Graphene Walls on Dielectric Substrates as Excellent Multifunctional Electrodes. *J. Mater. Chem. A* **2012**, *1*, 770-775.

(5) Kim, Y. S.; Joo, K.; Jerng, S. K.; Lee, J. H.; Moon, D.; Kim, J.; Yoon, E.; Chun, S. H. Direct Integration of Polycrystalline Graphene into Light Emitting Diodes by Plasma-assisted Metal-catalyst-free Synthesis. *ACS Nano* **2014**, *8*, 2230-2236.

(6) Kong, W. Y.; Wu, G. A.; Wang, K. Y.; Zhang, T. F.; Zou, Y. F.; Wang, D. D.; Luo, L. B. Graphene-β-Ga_2O_3 Heterojunction for Highly Sensitive Deep UV Photodetector Application. *Adv. Mater.* **2016**, *28*, 10725-10731.

(7) Liu, X.; Gu, L.; Zhang, Q.; Wu, J.; Long, Y.; Fan, Z. All-printable Band-edge Modulated ZnO Nanowire Photodetectors with Ultra-high Detectivity. *Nat. Commun.* **2014**, *5*, 4007.

(8) Chang, K. E.; Yoo, T. J.; Kim, C.; Kim, Y. J.; Lee, S. K.; Kim, S. Y.; Heo, S.; Min Kwon, G.; Lee, B. H. Gate-Controlled Graphene-Silicon Schottky Junction Photodetector. *Small* **2018**, *10*, 1801182.